Available online at www.sciencedirect.com
SCIENCE DIRECT®
Journal of Solid State Chemistry 179 (2006) 253–265
JOURNAL OF SOLID STATE CHEMISTRY
www.elsevier.com/locate/jssc

Influence of metal ions on the structures of Keggin polyoxometalate-based solids: Hydrothermal syntheses, crystal structures and magnetic properties

Zhenyu Shi[a], Jun Peng[a,*], Carlos J. Gómez-García[b], Samia Benmansour[b], Xiaojun Gu[a]

[a]*Institute of Polyoxometalate Chemistry, Faculty of Chemistry, Northeast Normal University, Changchun 130024, PR China*
[b]*Instituto de Ciencia Molecular, Universidad de Valencia. Pol. La Coma s/n 46980 Paterna, Valencia, Spain*

Received 20 May 2005; received in revised form 22 September 2005; accepted 24 September 2005
Available online 1 December 2005

Abstract

Three new Keggin polyoxometalate (POM)-based compounds linked to 3d metal complexes have been synthesized under hydrothermal conditions: $[Cu(phen)_2]_2\{[Cu(phen)]_2[SiMo_{12}O_{40}(VO)_2]\}$ (**1**), $\{[Zn(phen)_2]_2[GeMo_{12}O_{40}(VO)_2]\}\{[Zn(phen)_2(H_2O)]_2[GeMo_{12}O_{40}(VO)_2]\}\cdot 3H_2O$ (**2**) and $\{[Co(phen)_2]_2[PMo_{12}O_{40}(VO)_2]\}\{[Co(phen)_2(OH)]_2[PMo_{12}O_{40}(VO)_2]\}\cdot 2.5H_2O$ (**3**) (phen = 1,10-phenanthroline). These three compounds present, as building blocks, the bicapped Keggin anions $[XMo_{12}O_{40}(VO)_2]$ (X = Si, Ge and P). Compound **1** consists of a bicapped Keggin anion $[SiMo_{12}O_{40}(VO)_2]^{2-}$ linked to two $[Cu(phen)]^+$ complexes with two $[Cu(phen)_2]^+$ countercations. Compound **2** contains two bicapped Keggin anions $[GeMo_{12}O_{40}(VO)_2]^{4-}$, one linked to two $[Zn(phen)_2(H_2O)]^{2+}$ cations and the other one linked to two $[Zn(phen)_2]^{2+}$ cations. Compound **3** is a two-dimensional POM-based square network formed by bicapped Keggin anions $[PMo_{12}O_{40}(VO)_2]^{4-}$ connected by $[Co(phen)_2]^{2+}$ cations. Discrete bicapped Keggin anions $[PMo_{12}O_{40}(VO)_2]$ linked to two $[Co(phen)_2(OH)]^+$ cations are located between the layers. The magnetic properties show the presence of antiferromagnetic interactions among the reduced Mo(V) atoms (in the three compounds) plus a paramagnetic contribution from the V(IV) atoms (in **1** and **2**). Compound **3** shows, in addition, an antiferromagnetic interaction between the Co(II) and the V(IV) ions directly linked through an oxygen bridge. The low-temperature ESR spectra of compound **3** confirm the presence of the reduced Mo(V) ions and the antiferromagnetic coupling between the Co(II) and the V(IV) ions.

Keywords: Hydrothermal synthesis; Bicapped Keggin; Magnetic polyoxometalates

1. Introduction

Organic–inorganic hybrid materials have recently attracted great interest because of their diverse structural flexibility and potential applications in molecular absorption, biology, catalysis, photochemistry and magnetism [1,2]. An attractive challenge in this field is the design and synthesis of novel solid materials based on polyoxometalates (POMs). To date, several strategies have been successfully explored to design POM-based hybrid materials [2,3]. A number of transition metal coordination complex-linking POMs with zero-, one-, two- and three-dimensional frameworks have been reported accordingly [4] and there exists one example of a chain made with Keggin POMs directly connected by sharing one O atom [5]. Most of these compounds have been obtained from simple inorganic oxides or oxoanion salts. Although there are also several examples of POM-based compounds synthesized from POM precursors, the structural POM skeletons of the final species have changed under hydrothermal conditions [4c,4i–4k].

These scarce previous works show that Keggin POMs may be valuable building blocks since they can be directly used to prepare materials where the structural integrity of the POMs is maintained throughout the construction process (although with $(VO)^{2+}$ addition or metal exchange). This ability allows the control of the framework structure of

*Corresponding author. Fax: +86 431 568 4009.
E-mail addresses: jpeng@nenu.edu.cn, pjun56@yahoo.com (J. Peng).

0022-4596/$ - see front matter © 2005 Elsevier Inc. All rights reserved.
doi:10.1016/j.jssc.2005.09.051

the solid materials and may let the synthesis of POM-based materials with highly specific and cooperative functions. Furthermore, hydrothermal synthesis has become a powerful method for the preparation of organic–inorganic hybrid materials owing to its advantages over other methods (e.g., diffusion and sol–gel techniques), such as the effective use of inorganic and organic reagents with low solubility [6]. However, the problem for accurate prediction of crystal architectures under hydrothermal conditions remains unsolved and the understanding of hydrothermal reaction mechanism is still far behind, although it is usually described as self-assembly. Zubieta et al. [7] have systematically investigated the interplay of ligand geometries in the design of molybdenum oxoclusters-based hybrids. Li et al. [8] have reported the influence of the pH on the dimensionality of coordination polymers constructed from 3,5-pyrazoledicarboxylic acid. In contrast, studies of the influence of the metal ions on the structures of Keggin POM-based compounds under hydrothermal conditions are still rare.

In previous work, we have synthesized with hydrothermal methods several Keggin POM-based compounds, including a discrete cluster [9], a one-dimensional chain and a two-dimensional layer [10]. Our efforts are focused on the systematic study of the conditions that determine the structures of the final compounds, such as the presence of different metal ions and ligands that can link to the POMs or act as a bridge connecting them in the final structure. In this paper, we report the hydrothermal syntheses, structural characterization, and physical properties of three new POM-based compounds prepared from pre-formed Keggin POMs $[XMo_{12}O_{40}]^{n-}$ and different metal ions such as Cu(II), Zn(II) and Co(II): $[Cu^{I}(phen)_2]_2\{[Cu^{I}(phen)]_2[SiMo_{12}O_{40}(V^{IV}O)_2]\}$ (**1**), $\{[Zn(phen)_2]_2[GeMo_{12}O_{40}(V^{IV}O)_2]\}\{[Zn(phen)_2(H_2O)]_2[GeMo_{12}O_{40}(V^{IV}O)_2]\}\cdot 3H_2O$ (**2**) and $\{[Co(phen)_2]_2[PMo_{12}O_{40}(V^{IV}O)_2]\}\{[Co(phen)_2(OH)]_2[PMo_{12}O_{40}(V^{IV}O)_2]\}\cdot 2.5H_2O$ (**3**) (phen = 1,10-phenanthroline). Compound **1** contains one bicapped Keggin cluster linked to two $[Cu(phen)]^{+}$ complexes. Compound **2** consists of two bicapped Keggin clusters, one linked to two $[Zn(phen)_2]$ complexes and the other one linked to two $[Zn(phen)_2(H_2O)]^{2+}$ complexes. Compound **3** is a two-dimensional POM-based network intercalated by discrete bicapped Keggin anions linked to two $[Co(phen)_2(OH)]^{+}$ complexes. Interestingly, in contrast to previously reported POM-based hybrid materials, the intact Keggin skeletons in compounds **1–3** are still maintained without metal exchange (although with $(VO)^{2+}$ addition). Furthermore, they also constitute the first systematic study of the influence of the transition metal used (Cu^{2+}, Zn^{2+} or Co^{2+}) in the final structures of POM-based hybrid materials.

2. Experimental section

2.1. General procedures

All reagents were purchased commercially and used without further purification. Elemental analyses (C, H and N) were performed on a Perkin-Elmer 2400 CHN Elemental Analyzer. Cu, Zn, Co, Mo and V were determined by a Leaman inductively coupled plasma spectrometer. IR spectra were obtained on Alpha Centaurt FT/IR spectrometer with KBr pellets in the 400–4000 cm^{-1} region. XPS analyses were performed on a VG ESCALAB MK II spectrometer with a Mg$K\alpha$ (1253.6 eV) achromatic X-ray source. The vacuum inside the analysis chamber was maintained at 6.2×10^{-6} Pa during analysis. The TG analyses were performed on a Perkin-Elmer thermogravimetric analysis (TGA7) instrument in flowing N_2 with a heating rate of 10 °C min^{-1}. Cyclic voltammograms (CV) were obtained with a CHI 660 electrochemical workstation at room temperature. A platinum gauze was used as counterelectrode and an Ag/AgCl was used as reference electrode. A chemically bulk-modified carbon paste electrode (CPE) was used as working electrode. Variable temperature susceptibility measurements for the three compounds were carried out in the temperature range 2–300 K with an applied magnetic field of 0.1 T on polycrystalline samples with a Quantum Design MPMS-XL-5 SQUID magnetometer. The susceptibility data were corrected for the sample holder previously measured using the same conditions and for the diamagnetic contributions of the salt as deduced by using Pascal's constant tables (-1443×10^{-6}, -2424×10^{-6} and -2414×10^{-6} emu mol^{-1} for **1**, **2** and **3**, respectively). These diamagnetic corrections are similar to those obtained with the values estimated from the molecular weight (MW) approximation ($\chi_{dia}=-(MW/2)\cdot10^{-6}$ emu mol^{-1}) and correspond to room temperature $\chi_m T$ values of 0.43, 0.73 and 0.72 emu K mol^{-1} for **1**, **2** and **3**, respectively. Note that the temperature independent paramagnetism (TIP) cannot be accurately estimated from tabulated values. Nevertheless, from magnetic measurements on diamagnetic Keggin anions we can estimate a TIP contribution of ca. 10^{-3} emu mol^{-1} for each Keggin unit. Therefore, the corrected TIP contributions are 10^{-3} emu mol^{-1} for compound **1** and 2×10^{-3} emu mol^{-1} for compounds **2** and **3** (neglecting the TIP contributions of the paramagnetic centers which are about two orders of magnitude lower). With these corrections we consider that the error in the $\chi_m T$ values at room temperature is not higher than 0.3 emu K mol^{-1} and, therefore, that the differences between the expected and observed room temperature $\chi_m T$ values (see magnetic section) are clearly significant since they are well above this value (0.65, 2.5 and 1.6–4.6 emu K mol^{-1} for **1**, **2** and **3**, respectively). Isothermal magnetizations were performed in the same samples at 2 K with applied magnetic fields of up to 5 T. Q-band ESR spectra of compound **3** were recorded on a polycrystalline sample with a Bruker E-500 ELEXSYS spectrometer in the temperature range 300–5 K.

2.2. Syntheses

$[Cu^{I}(phen)_2]_2\{[Cu^{I}(phen)]_2[SiMo_{12}O_{40}(V^{IV}O)_2]\}$ (**1**): The starting materials: $H_4[SiMo_{12}O_{40}]\cdot xH_2O$ [11] (0.25 mmol), $Cu(NO_3)_2\cdot3H_2O$ (0.25 mmol), NH_4VO_3 (0.5 mmol), phen (0.25 mmol), triethylamine (1.0 mmol) and H_2O (9 mL)

were mixed in a molar ratio 1:1:2:1:4:2000. The resulting suspension was stirred for 1 h, sealed in an 18 mL Teflon-lined reactor and heated at 165 °C for 6 days. Then the autoclave was cooled at 5 °C h^{-1} to room temperature. Black block crystals of **1** were filtered, washed with water, and dried (yield 69%, based on molybdenum). $C_{72}H_{48}Cu_4Mo_{12}N_{12}O_{42}SiV_2$ (3288.63) **1**: Calcd. C 26.29, H 1.47, N 5.11, Cu 7.73, Mo 35.01, V 3.10; found C 26.23, H 1.39, N 5.20, Cu 7.86, Mo 35.11, V 2.99.

$\{[Zn(phen)_2]_2[GeMo_{12}O_{40}(V^{IV}O)_2]\}\{[Zn(phen)_2(H_2O)]_2[GeMo_{12}O_{40}(V^{IV}O)_2]\}\cdot 3H_2O$ (**2**): The procedure is similar to that described for the preparation of **1**, except that $H_4[SiMo_{12}O_{40}]\cdot xH_2O$ was replaced by $H_4[GeMo_{12}O_{40}]\cdot xH_2O$ [11] (yield 58%, based on molybdenum). $C_{96}H_{70}Ge_2Mo_{24}N_{16}O_{89}V_4Zn_4$ (5784.28) **2**: Calcd. C 19.93, H 1.21, N 3.88, Zn 4.52, Mo 39.81, V 3.52; found C 20.04, H 1.16, N 3.95, Zn 4.63, Mo 39.69, V 3.58.

$\{[Co(phen)_2]_2[PMo_{12}O_{40}(V^{IV}O)_2]\}\{[Co(phen)_2(OH)]_2[PMo_{12}O_{40}(V^{IV}O)_2]\}\cdot 2.5H_2O$ (**3**): The procedure is similar to that described for the preparation of **1**, except that $H_4[SiMo_{12}O_{40}]\cdot xH_2O$ was replaced by $H_3[PMo_{12}O_{40}]\cdot xH_2O$ [11] (yield 66%, based on molybdenum). $C_{96}H_{70}Co_4Mo_{24}N_{16}P_2O_{88.5}V_4$ (5667.08) **3**: Calcd. C 20.34, H 1.24, N 3.96, Co 4.16, Mo 40.63, V 3.60; found C 20.23, H 1.19, N 4.07, Co 4.28, Mo 40.51, V 3.66.

Preparation of 1-CPE, 2-CPE and 3-CPE: 100 mg graphite powder and ca. 20 mg of compound **1** (**2** or **3**) were mixed and ground together in an agate mortar to achieve a homogeneous dry mixture. After addition of 0.2 mL of nujol, the mixture was stirred with a glass rod. The homogenized mixture was inserted in a 3 mm inner diameter glass tube. Electrical contact was established with copper rod through the back of the electrode.

2.3. X-ray crystallography

Crystal data for compounds **1** and **2** were collected on a Rigaku R-AXIS RAPID IP diffractometer, while the measurement for compound **3** was performed on a Bruker SMART-CCD diffractometer, with Mo*K*α monochromated radiation ($\lambda = 0.71073$ Å) at 293 K. All the structures were solved by directed methods and refined by full-matrix least squares on F^2 using the SHELXTL crystallographic software package. All the non-hydrogen atoms were refined anisotropically. The positions of hydrogen atoms on carbon atoms were calculated theoretically. The crystal data and structure refinement of compounds **1**–**3** are summarized in Table 1. Selected bond lengths and angles are listed in Tables 2–4. CCDC reference numbers are 265898, 261262 and 261263 for compounds **1**, **2** and **3**, respectively.

3. Results and discussion

3.1. Crystal structures

$[Cu^I(phen)_2]_2\{[Cu^I(phen)]_2[SiMo_{12}O_{40}(V^{IV}O)_2]\}$ (1): X-ray single-crystal diffraction reveals that compound **1** contains a bicapped Keggin anion $[SiMo_8^{VI}Mo_4^{V}O_{40}(V^{IV}O)_2]^{4-}$ linked to two $[Cu^I(phen)]$ complexes to give the anion $\{[Cu^I(phen)]_2[SiMo_8^{VI}Mo_4^{V}O_{40}(V^{IV}O)_2]\}^{2-}$ and two $[Cu(phen)_2]^+$ counterions (Fig. 1). The bicapped Keggin

Table 1
Crystal data and structure refinement for compounds **1**, **2** and **3**

Compounds	**1**	**2**	**3**
Empirical formula	$C_{72}H_{48}Cu_4Mo_{12}N_{12}O_{42}SiV_2$	$C_{96}H_{70}Ge_2Mo_{24}N_{16}O_{89}V_4Zn_4$	$C_{96}H_{70}Co_4Mo_{24}N_{16}P_2O_{88.5}V_4$
Formula weight	3288.63	5784.28	5667.08
Temperature (K)	293	293	293
Crystal system	Triclinic	Monoclinic	Monoclinic
Space group	$P\bar{1}$	$P2_1/c$	$P2_1/c$
a (Å)	13.380(3)	21.428(4)	21.8258(2)
b (Å)	14.084(3)	16.567(3)	16.5164(1)
c (Å)	14.742(3)	21.205(4)	21.1988(2)
α (deg)	111.46(3)	90	90
β (deg)	116.63(3)	99.69(3)	100.5050(1)
γ (deg)	90.25(3)	90	90
V (Å^3)	2263.6(8)	7420(3)	7513.7(1)
Z	1	2	2
λ (Å)	0.71073	0.71073	0.71073
Dc/Mg (m^{-1})	2.412	2.586	2.502
μ (mm^{-1})	2.822	2.710	2.703
F(000)	1580	5496	5396
Reflection collected	15429	52549	40794
Independent reflections	9916	13290	14714
Absorption correction	Empirical	Empirical	Empirical
Refinement method	Full-matrix least-squares on F^2	Full-matrix least-squares on F^2	Full-matrix least-squares on F^2
R_1, wR_2 [$I>2\sigma(I)$]	0.0654, 0.1370	0.0799, 0.1449	0.0664, 0.1777
R_1, wR_2 (all data)	0.0837, 0.1447	0.1122, 0.1557	0.0846, 0.1906

Table 2
Selected bond lengths (Å) and angles (deg) for compound **1**

Atoms	Dist. (Å)	Atoms	Dist. (Å)
Cu(1)–O(14)	1.868(5)	Mo(1)–O(16)	1.635(6)
Cu(1)–N(2)	1.981(6)	Mo(1)–O(7)#	1.913(7)
Cu(1)–N(1)	2.070(7)	Mo(1)–O(8)#	1.917(7)
Cu(2)–N(5)	2.059(8)	Mo(1)–O(18)	1.926(7)
Cu(2)–N(3)	2.015(7)	Mo(1)–O(20)	1.930(7
Cu(2)–N(4)	2.056(8)	Mo(1)–O(4)#	2.395(9)
Cu(2)–N(6)	2.023(7)	Mo(1)–O(1)#	2.494(10)
V(1)–O(14)	1.616(5)	Mo(2)–V(1)	3.0774(15)
V(1)–O(12)	1.923(6)	Mo(2)–O(3)#	2.467(10)
V(1)–O(15)	1.926(6)	Mo(2)–O(4)	2.401(9)
V(1)–O(17)	1.937(6)	Mo(2)–O(12)	2.033(6)
V(1)–O(11)	1.944(6)	Mo(2)–O(15)	2.022(6)
Si(1)–O(1)	1.608(9)	Mo(2)–O(22)	1.824(7)
Si(1)–O(2)	1.614(8)	Mo(2)–O(7)	1.814(7)
Si(1)–O(3)#	1.627(9)	Mo(2)–O(23)	1.649(6)
Si(1)–O(4)#	1.675(9)		
Atoms	Angle (deg)	Atoms	Angle (deg)
O(14)–Cu(1)–N(2)	162.1(3)	O(16)–Mo(1)–O(7)#	100.7(4)
O(14)–Cu(1)–N(1)	114.9(3)	O(16)–Mo(1)–O(8)#	102.1(4)
N(2)–Cu(1)–N(1)	83.0(3)	O(16)–Mo(1)–O(18)	101.0(4)
N(3)–Cu(2)–N(6)	142.8(3)	O(7)#–Mo(1)–O(18)	89.4(4)
N(3)–Cu(2)–N(4)	82.2(3)	O(8)#–Mo(1)–O(18)	156.9(5)
N(6)–Cu(2)–N(4)	110.7(3)	O(16)–Mo(1)–O(20)	101.6(4)
N(3)–Cu(2)–N(5)	120.6(3)	O(7)#–Mo(1)–O(20)	157.6(5)
N(6)–Cu(2)–N(5)	81.4(3)	O(18)–Mo(1)–O(20)	86.1(3)
N(4)–Cu(2)–N(5)	125.0(3)	O(7)#–Mo(1)–O(4)#	63.0(4)
O(1)–Si(1)–O(2)	110.5(5)	O(20)–Mo(1)–O(1)#	63.7(3)
O(1)–Si(1)–O(3)#	110.4(5)	O(23)–Mo(2)–O(7)	101.9(4)
O(2)–Si(1)–O(3)#	111.7(5)	O(23)–Mo(2)–O(22)	101.2(4)
O(3)#–Si(1)–O(4)#	106.9(5)	O(23)–Mo(2)–O(15)	100.5(3)
O(14)–V(1)–O(12)	114.0(3)	O(22)–Mo(2)–O(15)	156.0(4)
O(14)–V(1)–O(15)	113.4(3)	O(23)–Mo(2)–O(12)	99.2(3)
O(12)–V(1)–O(15)	80.1(3)	O(15)–Mo(2)–O(12)	75.3(2)
O(14)–V(1)–O(17)	115.8(3)	O(7)–Mo(2)–O(4)	64.0(4)
O(12)–V(1)–O(17)	130.2(3)	O(23)–Mo(2)–O(3)#	155.0(3)
O(15)–V(1)–O(17)	80.0(3)	O(12)–Mo(2)–O(4)	92.7(3)
O(14)–V(1)–O(11)	116.6(3)	O(7)–Mo(2)–O(3)#	99.5(5)
O(15)–V(1)–O(11)	130.0(4)		

Symmetry transformations used to generate equivalent atoms: #1 $-x+1$, $-y+1$, $-z$.

Table 3
Selected bond lengths (Å) and angles (deg) for compound **2**

Atoms	Dist. (Å)	Atoms	Dist. (Å)
Zn(1)–O(45)	2.053(9)	Zn(2)–N(6)	2.147(9)
Zn(1)–N(2)	2.085(12)	V(1)–O(45)	1.629(9)
Zn(1)–N(4)	2.093(7)	V(1)–O(20)	1.906(12)
Zn(1)–N(3)	2.101(8)	V(1)–O(14)	1.916(9)
Zn(1)–N(1)	2.120(12)	V(1)–O(35)	1.920(10)
Zn(1)–OW3	2.21(3)	V(1)–O(43)	1.935(11)
Zn(2)–N(5)	2.075(8)	V(2)–O(34)	1.624(9)
Zn(2)–N(7)	2.077(13)	V(2)–O(37)	1.914(10)
Zn(2)–O(34)	2.087(9)	V(2)–O(18)	1.914(10)
Zn(2)–N(8)	2.133(12)	V(2)–O(30)	1.921(9)
V(2)–O(24)	1.925(10)	Ge(1)–O(5)	1.781(15)
V(2)–Mo(11)	3.110(3)	Ge(2)–O(48)	1.671(18)
Ge(1)–O(61)	1.698(15)	Ge(2)–O(1)	1.732(15)
Ge(1)–O(40)	1.706(16)	Ge(2)–O(47)	1.767(16)
Ge(1)–O(8)	1.764(15)	Ge(2)–O(7)	1.784(16)
Atoms	Angle (deg)	Atoms	Angle (deg)
O(45)–Zn(1)–N(2)	97.3(4)	O(34)–Zn(2)–N(8)	96.0(4)
O(45)–Zn(1)–N(4)	91.4(4)	N(5)–Zn(2)–N(6)	77.6(4)
N(2)–Zn(1)–N(4)	106.4(4)	N(7)–Zn(2)–N(6)	96.3(4)
O(45)–Zn(1)–N(3)	157.5(4)	O(34)–Zn(2)–N(6)	169.1(4)
N(2)–Zn(1)–N(3)	104.9(4)	N(8)–Zn(2)–N(6)	91.8(4)
N(4)–Zn(1)–N(3)	78.9(4)	O(45)–V(1)–O(20)	115.3(6)
O(45)–Zn(1)–N(1)	89.1(4)	O(45)–V(1)–O(14)	114.5(6)
N(2)–Zn(1)–N(1)	79.3(5)	O(20)–V(1)–O(14)	79.6(5)
N(4)–Zn(1)–N(1)	174.1(4)	O(45)–V(1)–O(35)	113.5(5)
N(3)–Zn(1)–N(1)	98.6(4)	O(20)–V(1)–O(35)	131.2(6)
O(45)–Zn(1)–OW3	90.3(8)	O(14)–V(1)–O(35)	80.8(4)
N(2)–Zn(1)–OW3	169.0(10)	O(45)–V(1)–O(43)	113.9(6)
N(4)–Zn(1)–OW3	81.2(9)	O(20)–V(1)–O(43)	80.5(5)
N(3)–Zn(1)–OW3	68.3(8)	O(14)–V(1)–O(43)	131.6(7)
N(1)–Zn(1)–OW3	92.9(9)	O(35)–V(1)–O(43)	80.2(5)
N(5)–Zn(2)–N(7)	111.0(4)	O(34)–V(2)–O(37)	113.7(6)
N(5)–Zn(2)–O(34)	93.3(4)	O(34)–V(2)–O(18)	116.6(6)
N(7)–Zn(2)–O(34)	92.5(4)	O(37)–V(2)–O(18)	129.7(6)
N(5)–Zn(2)–N(8)	165.1(4)	O(34)–V(2)–O(30)	115.4(5)
N(7)–Zn(2)–N(8)	80.4(5)	O(37)–V(2)–O(30)	79.7(4)
O(18)–V(2)–O(30)	78.9(4)	V(2)–O(34)–Zn(2)	155.1(6)
O(34)–V(2)–O(24)	114.7(5)	V(1)–O(45)–Zn(1)	142.2(6)
O(37)–V(2)–O(24)	79.7(5)	O(8)–Ge(1)–O(5)	104.7(7)
O(18)–V(2)–O(24)	80.3(5)	O(48)–Ge(2)–O(1)	68.1(8)
O(30)–V(2)–O(24)	129.9(5)	O(48)–Ge(2)–O(47)	69.5(8)
O(61)–Ge(1)–O(40)	69.0(8)	O(1)–Ge(2)–O(47)	110.5(8)
O(61)–Ge(1)–O(8)	114.8(8)	O(48)–Ge(2)–O(7)	67.4(8)
O(40)–Ge(1)–O(8)	70.8(7)	O(1)–Ge(2)–O(7)	106.3(7)
O(61)–Ge(1)–O(5)	107.1(8)	O(47)–Ge(2)–O(7)	104.8(8)
O(40)–Ge(1)–O(5)	70.2(7)		

anion $[SiMo_8^{VI}Mo_4^{V}O_{40}(V^{IV}O)_2]^{4-}$ can be described as an α-Keggin core $\{SiMo_{12}O_{40}\}$ with two $\{VO\}$ units, linked to four oxygen atoms of two opposite $\{Mo_4O_4\}$ square holes in the Keggin structure. The Keggin anions present a T_d symmetry and consist of four internally edge-shared octahedral triads $\{Mo_3O_{13}\}$, connected with each other by corner-sharing oxygen atoms and encapsulating a central XO_4 tetrahedron (X = Si in **1**, Ge in **2** and P in **3**). These bicapped Keggin-type anions are similar to those found in $[SiMo_{10}V_2^{IV}O_{40}(V^{IV}O)_2]^{4-}$ [12] and $[PMo_6^{V}Mo_6^{VI}O_{40}(V^{IV}O)_2]^{5-}$ [13]. There is only one crystallographically unique vanadium atom, exhibiting a distorted $\{VO_5\}$ square pyramidal environment. The axial position is occupied by the oxygen atom of the VO group and the basal plane is formed by the four POM oxygen atoms. In all the bicapped Keggin anions of the three compounds, the axial V–O bond distances are shorter than the four basal V–O distances and the vanadium atoms are above the basal plane. Thus, the O_{axial}–V–O_{basal} bond angles are larger than 90° whereas the *cis* O_{basal}–V–O_{basal} bond angles are smaller than 90°. All molybdenum atoms have a distorted $\{MoO_6\}$ octahedral environment and, according to the kind of oxygen atom bound to the molybdenum atoms, the Mo–O bond distances are divided in three categories. The Mo–O_c bond distances (O_c = center oxygen atom) are the longest ones, the Mo–O_b bond distances (O_b = bridge oxygen atom) are intermediate and the Mo–O_t bond

Table 4
Selected bond lengths (Å) and angles (deg) for compound **3**

Atoms	Dist. (Å)	Atoms	Dist. (Å)
Co(1)–O(21)	2.063(7)	V(1)–O(28)	1.916(8)
Co(2)–N(5)	2.137(9)	P(1)–O(43)	1.509(13)
V(2)–O(23)	1.937(7)	Co(1)–N(3)	2.128(9)
Co(1)–N(1)	2.100(10)	V(1)–O(26)	1.923(9)
Co(2)–O(31)	2.236(7)	P(1)–O(9)	1.524(12)
V(2)–O(27)	1.937(7)	Co(1)–OW1	2.143(9)
Co(1)–N(4)	2.120(10)	V(1)–O(29)	1.925(8)
V(1)–O(21)	1.648(7)	P(1)–O(44)	1.627(11)
P(1)–O(42)	1.504(14)	Co(2)–O(35)#1	2.054(7)
Co(1)–N(2)	2.119(9)	V(1)–O(30)	1.927(8)
P(2)–O(45)	1.506(12)	V(2)–O(33)	1.926(7)
Co(2)–N(8)	2.095(9)	P(2)–O(46)	1.530(12)
V(2)–O(35)	1.651(6)	Co(2)–N(6)	2.105(10)
P(2)–O(41)	1.518(11)	V(2)–O(32)	1.929(7)
Co(2)–N(7)	2.099(9)	P(2)–O(37)	1.611(12)
Atoms	**Angle (deg)**	**Atoms**	**Angle (deg)**
O(21)–Co(1)–N(1)	169.7(3)	N(5)–Co(2)–O(31)	94.5(3)
N(8)–Co(2)–N(5)	175.2(4)	O(42)–P(1)–O(9)	110.7(7)
O(33)–V(2)–O(23)	80.6(3)	N(4)–Co(1)–N(3)	78.2(4)
O(21)–Co(1)–N(4)	94.8(3)	O(21)–V(1)–O(28)	112.5(4)
N(7)–Co(2)–N(5)	97.7(4)	O(43)–P(1)–O(9)	113.3(7)
O(32)–V(2)–O(23)	79.6(3)	N(2)–Co(1)–N(3)	177.1(4)
N(1)–Co(1)–N(4)	93.5(4)	O(21)–V(1)–O(26)	114.5(5)
N(6)–Co(2)–N(5)	79.0(4)	O(42)–P(1)–O(44)	73.2(7)
O(35)–V(2)–O(27)	113.3(4)	O(21)–Co(1)–OW1	90.0(3)
O(21)–Co(1)–N(2)	93.4(3)	O(28)–V(1)–O(26)	80.7(4)
O(35)#1–Co(2)–O(31)	94.5(3)	O(43)–P(1)–O(44)	74.2(7)
O(33)–V(2)–O(27)	80.5(3)	N(1)–Co(1)–OW1	82.4(4)
N(1)–Co(1)–N(2)	79.4(4)	O(21)–V(1)–O(29)	115.9(4)
N(8)–Co(2)–O(31)	82.7(3)	O(9)–P(1)–O(44)	72.7(7)
O(32)–V(2)–O(27)	80.1(3)	N(4)–Co(1)–OW1	172.2(4)
N(4)–Co(1)–N(2)	99.0(4)	O(28)–V(1)–O(29)	131.6(4)
N(7)–Co(2)–O(31)	87.4(3)	O(45)–P(2)–O(41)	67.9(6)
O(23)–V(2)–O(27)	132.2(4)	N(2)–Co(1)–OW1	86.8(4)
O(21)–Co(1)–N(3)	86.1(3)	O(26)–V(1)–O(29)	79.8(4)
N(6)–Co(2)–O(31)	173.2(3)	O(45)–P(2)–O(46)	113.7(7)
O(42)–P(1)–O(43)	112.4(7)	N(3)–Co(1)–OW1	96.0(4)
N(1)–Co(1)–N(3)	101.5(4)	O(21)–V(1)–O(30)	112.6(4)
O(41)–P(2)–O(46)	70.5(6)	O(46)–P(2)–O(37)	73.8(6)
O(35)#1–Co(2)–N(8)	91.4(4)	(35)#1–Co(2)–N(6)	88.0(3)
O(28)–V(1)–O(30)	81.6(3)	O(35)–V(2)–O(33)	113.0(4)
O(45)–P(2)–O(37)	72.6(6)	V(1)–O(21)–Co(1)	140.8(4)
O(35)#1–Co(2)–N(7)	169.1(4)	N(8)–Co(2)–N(6)	103.6(4)
O(26)–V(1)–O(30)	133.0(5)	O(35)–V(2)–O(32)	116.8(4)
O(41)–P(2)–O(37)	107.6(6)	V(2)–O(35)–Co(2)#2	160.7(4)
N(8)–Co(2)–N(7)	78.2(4)	N(7)–Co(2)–N(6)	91.3(4)
O(29)–V(1)–O(30)	80.3(3)	O(33)–V(2)–O(32)	130.2(3)
Mo7–O31–Co2	144.2(4)	O(35)#1–Co(2)–N(5)	92.8(3)
O(35)–V(2)–O(23)	114.5(4)		

Symmetry transformations used to generate equivalent atoms: #1 x, $-y+3/2$, $z+1/2$ #2 x, $-y+3/2$, $z-1/2$.

distances (O_t = terminal oxygen atom) are the shortest ones. The SiO_4 tetrahedron located in the center of the host cage is disordered. Thus, each Si atom is surrounded by eight oxygen atoms, each with an occupancy factor of 50%, in the vertex of a distorted cube. The Si–O bond distances are in the ranges 1.608(9)–1.675(9) Å. The bond valence sum (BVS) calculations [14] show that the oxidation state of the two vanadium atoms is +4 (average calculated value = 4.21) and that there are four Mo(V) atoms and eight Mo(VI) atoms (the average calculated value is 5.73, compared to an expected value of 5.67).

There are two types of coordination environments for the Cu(I) ions in compound **1**: Cu1, which is connected to the POM, exhibits a triangular coordination environment formed by the bridging oxygen atom, O14, from the $(VO)^{2+}$ group of the POM (Cu1–O14 = 1.868(5) Å) and by two N atoms (N1, N2) from one phenanthroline ligand (Cu1–N1 = 2.070(7) Å, Cu1–N2 = 1.981(6) Å). The O14–Cu1–N1, O14–Cu1–N2 and N2–Cu1–N1 bond angles are 114.9(3)°, 162.1(3)° and 83.0(3)°, respectively. Cu2, located in the isolated cationic complex $[Cu(phen)_2]^+$, presents a distorted tetrahedral geometry formed by four N atoms (N3, N4, N5 and N6) from two phenanthroline ligands (Cu2–N, 2.015(7)–2.059(1) Å; N–Cu2–N, 81.4(3)–142.8(3)°).

Our former work has demonstrated that using as building blocks POMs with different redox properties, such as $H_4SiMo_{12}O_{40}$ or $H_4GeMo_{12}O_{40}$, does not produce significant changes on the POM-based extended solids. However, the change of the Cu^{2+} cations in **1** by Zn^{2+} cations may induce novel structural arrangements (as proved with compound **2**), since Cu^{2+} cation is easily reduced to Cu^+ cation by organic amine under hydrothermal conditions while Zn^{2+} cation is very stable and will not be reduced in these conditions. On the other hand, Cu^+ cations, with d^{10} configuration, tend to form triangular, tetrahedral and square-pyramidal geometries, whereas Zn^{2+} cations have a tendency to generate octahedral, trigonal-bipyramidal, square-pyramidal or tetrahedral coordination geometries, as observed in compound **2**.

$\{[Zn(phen)_2]_2[GeMo_{12}O_{40}(V^{IV}O)_2]\}\{[Zn(phen)_2(H_2O)]_2[GeMo_{12}O_{40}(V^{IV}O)_2]\}\cdot 3H_2O$ (2). X-ray single-crystal diffraction reveals that compound **2** contains two crystallographically independent neutral bicapped Keggin clusters, namely, $[Zn(phen)_2(H_2O)]_2[GeMo_8^{VI}Mo_4^{V}O_{40}(V^{IV}O)_2]$ (cluster A, Fig. 2a) and $[Zn(phen)_2]_2[GeMo_8^{VI}Mo_4^{V}O_{40}(V^{IV}O)_2]$ (cluster B, Fig. 2b). As shown in Fig. 2, both clusters are very similar: they contain a bicapped Keggin POM linked to two cationic bis(phenanthroline)zinc(II) complexes. Both bicapped Keggin POMs are very similar to that found in compound **1** (see above). The only difference deals with the central atom (Si in **1** and Ge in **2**). As in compound **1**, the BVS calculations [14] show that in both clusters of compound **2** the oxidation state of all the vanadium atoms is +4 (average calculated value = 4.30), four molybdenum atoms are in the +5 oxidation state, while the other eight molybdenum atoms are in the +6 oxidation state (the average calculated value is 5.76, compared to an expected value of 5.67).

When comparing clusters A and B, we notice that the only difference deals with the Zn(II) complexes linked to the bicapped Keggin units: in cluster B the Zn(II) complex is $[Zn(phen)_2]^{2+}$ whereas in cluster A the Zn(II) complex

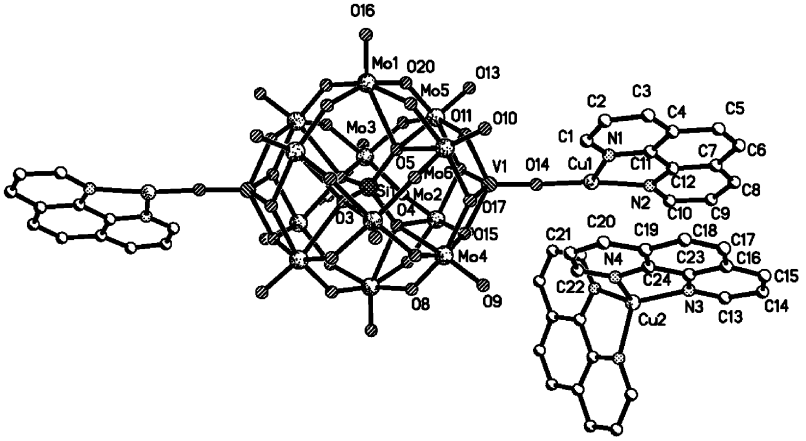

Fig. 1. Structure of the $[Cu(phen)_2]^+$ cation and the $\{[Cu(phen)]_2[SiMo_{12}O_{40}(VO)_2]\}^{2-}$ anion in compound **1**.

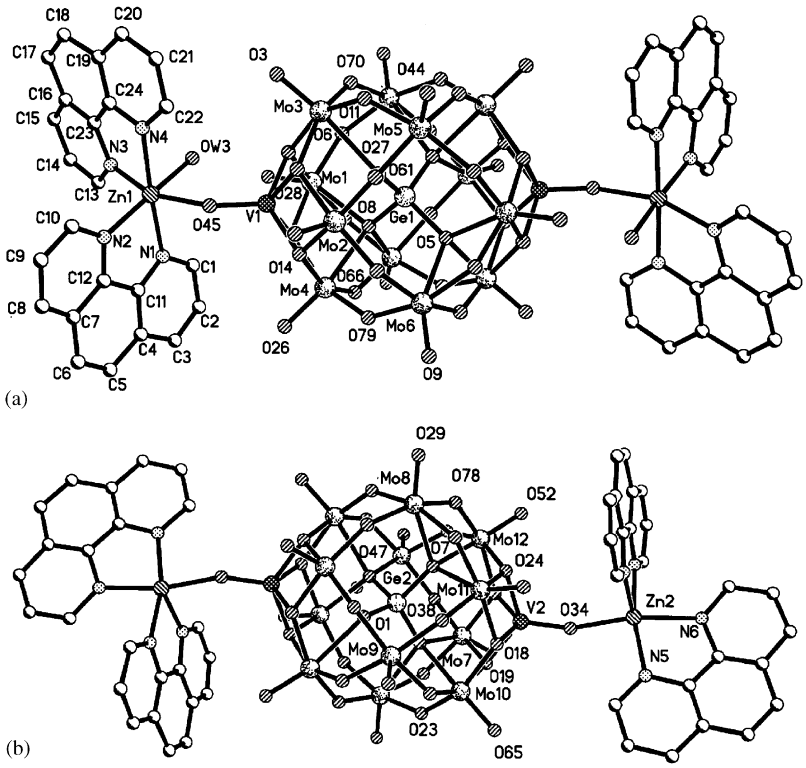

Fig. 2. Structure of compound **2**: (**a**) cluster A: $[Zn(phen)_2(H_2O)]_2[GeMo_{12}O_{40}(VO)_2]$ and (**b**) cluster B: $[Zn(phen)_2]_2[GeMo_{12}O_{40}(V^{IV}O)_2]$.

presents an additional coordinated water molecule: $[Zn(phen)_2(H_2O)]^{2+}$. Thus, the $[Zn(phen)_2(H_2O)]^{2+}$ complex in cluster A (Fig. 2a) presents a distorted octahedral geometry defined by the bridging oxygen atom (Zn1–O45 = 2.053(9) Å), a water molecule (Zn1–O3W = 2.21(3) Å) *cis* to the bridging O45 atom and four N atoms from two phenantroline ligands (N1–N4) with very similar Zn1–N bond distances (2.085(12)–2.120(12) Å). As expected for an octahedral geometry, all the *cis* angles are close to 90° (68.3(8)–106.4(4)°) and the three *trans* angles are close to 180° (157.5(4)°, 169.0(10)° and 174.1(4)°). The bridge between the POM and the Zn(II) ion deviates from linearity (V1–O45–Zn1 = 142.2(6)°). The $[Zn(phen)_2]^{2+}$ complex in cluster B (Fig. 2b) presents a distorted square pyramidal geometry with the bridging oxygen atom, O34 and three N atoms (N5, N6 and N8) from the phenanthroline ligands in the basal plane (Zn2–O34 = 2.087(9), Zn2–N5 = 2.075(8) Å, Zn2–N6 = 2.147(9) Å and Zn2–N8 = 2.133(12) Å). The other N atom (N7) occupies the axial position (Zn2–N7 = 2.077(13) Å). The *cis* O–Zn–N bond angles within the basal plane are close to 90° (93.3(4)° and 96.0(4)°) whereas the *trans* O–Zn–N bond angle is close to 180° (169.1(4)°). The distortion from the square pyramidal geometry is shown by one of the four bond angles between the axial N atom (N7) and the basal O and N coordinated atoms. Thus, three of them are close to 90° (80.4(5)°,

92.5(4)° and 96.3(4)°) but one significantly deviates from 90° (111.0(4)°). As in cluster A (see above), the POM-cation bridge in cluster B also deviates from linearity (V2–O34–Zn2 = 155.1(6)°).

Compared with Cu^{+} and Zn^{2+} cations, Co^{2+} cation presents a d^7 configuration with a marked tendency to form octahedral complexes that may act as bridging units between the POMs units; therefore, the change of Cu^{+} or Zn^{2+} cations by Co^{2+} may induce significant differences in the structure of the final POM-based compounds, as can be observed in compound **3**.

$\{[Co(phen)_2]_2[PMo_{12}O_{40}(V^{IV}O)_2]\}\{[Co(phen)_2(OH)]_2[PMo_{12}O_{40}(V^{IV}O)_2]\}\cdot 2.5H_2O$ (3): X-ray single-crystal diffraction shows that the structure of compound **3** is very similar to those of $\{[Co(phen)_2]_2[SiMo_{12}O_{40}(VO)_2]\}\{[Co(phen)_2(H_2O)]_2[SiMo_{12}O_{40}(VO)_2]\}\cdot 3H_2O$, very recently published [10], and $\{[Co(phen)_2(H_2O)]_2[PMo_{10}V_4O_{42}]\}\{[Co(phen)_2]_2[PMo_{10}V_4O_{42}]\}\cdot 4H_2O$, reported during the preparation of this manuscript [4j]. Nevertheless, this last compound has been prepared from a pre-formed Dawson–Wells $H_6P_2Mo_{18}O_{62}$ POM (compared to a Keggin POM in compound **3**) and presents a different V/Mo ratio (4/10, compared to 2/12 in **3**).

Compound **3** presents layers made of water molecules and discrete clusters formed by bicapped Keggin POMs linked to two cobalt complexes (layer I) (Figs. 3a and 4a) alternating with layers formed by bicapped Keggin POMs connected by four cobalt complexes in a square lattice (layer II) (Figs. 3b and 4b). The BVS calculations [14] show that in both bicapped Keggin POMs of compound **3** the oxidation state of all the vanadium atoms is +4 (average calculated value = 4.14). For the molybdenum atoms, the BVS calculations show an average value of 5.74, which is in between the expected values for Mo(V)/Mo(VI) ratios of 4/8 and 3/9 (5.67 and 5.75, respectively). Assuming that the oxidation state of the cobalt ions is +2 in the four bis(phen) complexes per formula unit, and that the oxygen atom bound to the Co(II) atoms in layer I is an OH^{-} anion, then the average Mo(V)/(Mo(VI) ratio must be 4/8. Note that if the OH^{-} anions in layer I were water

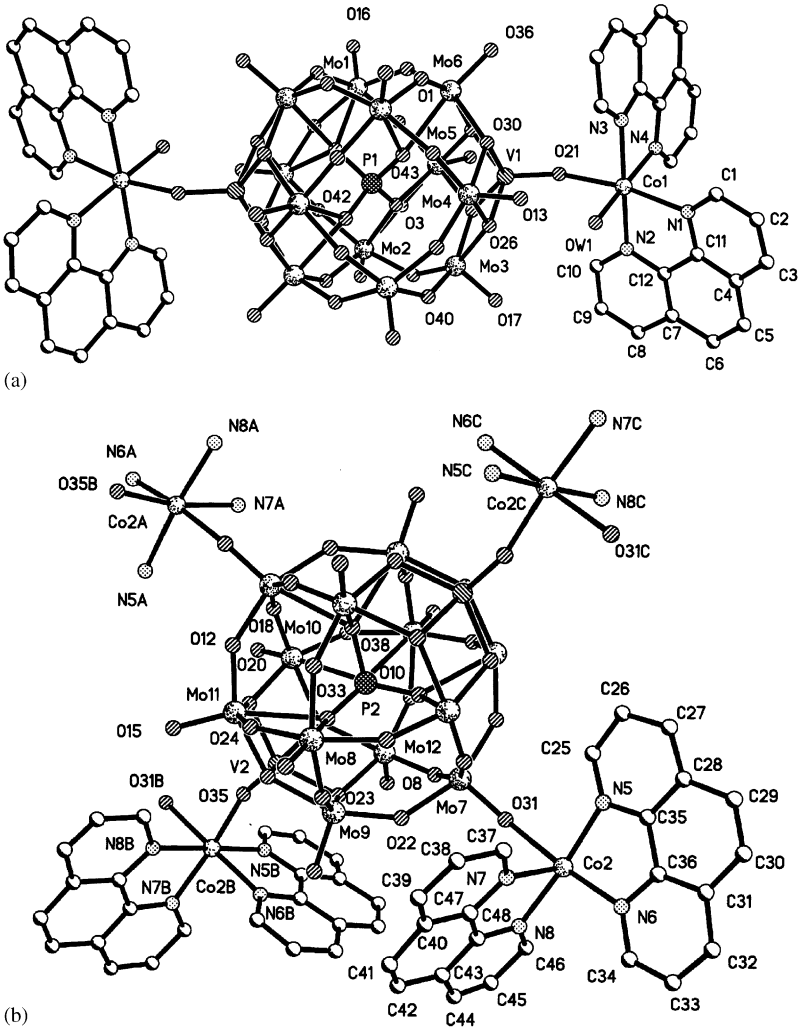

Fig. 3. Structure of compound **3**: (**a**) the discrete units $[Co(phen)_2(OH)]_2[PMo_{12}O_{40}(VO)_2]$ in layer I and (**b**) the $[PMo_{12}O_{40}(VO)_2]$ units linked to four $[Co(phen)_2]$ complexes in layer II. The carbon and hydrogen atoms of two phenantroline ligands have been omitted for clarity.

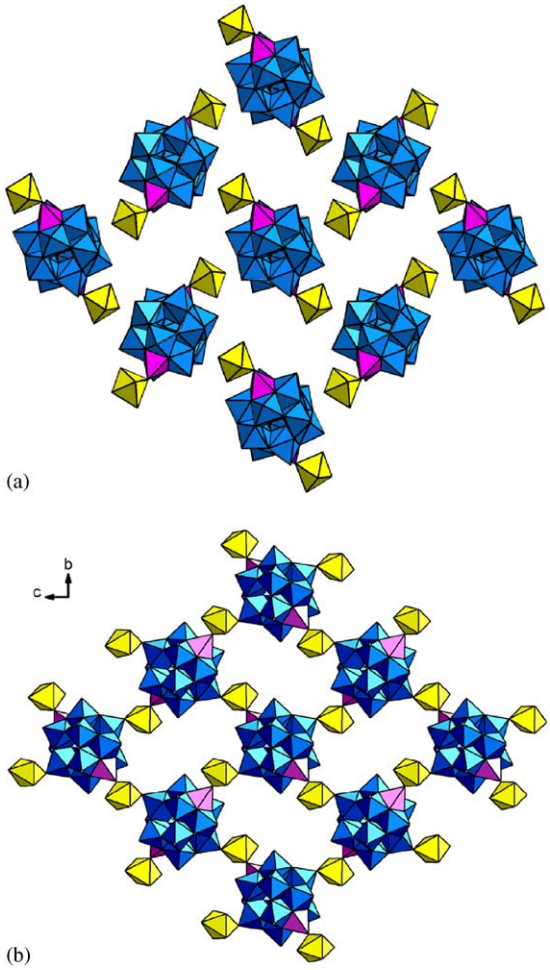

Fig. 4. Polyhedral representation, on the *bc* plane, in compound **3** of (**a**) the discrete layer I and (**b**) the 2D layer II. All carbon and hydrogen atoms and the water molecules are omitted for clarity.

molecules, then the average Mo(V)/Mo(VI) ratio should be 5/7, whose expected average value (5.58) is far from the calculated one (5.74). Furthermore, there are two recently reported POM-based hybrid compounds that present $[M(\text{phen})_2(\text{OH})]^+$ complexes (M^{II} = Co and Ni) linked to bicapped Keggin POMs units [4k]. Therefore, we assume that the average Mo(V)/(Mo(VI) ratio is 4/8. This value leads to two possible charge distributions in the POM clusters: (1) $Mo_3^{V}Mo_9^{VI}$ in one POM and $Mo_5^{V}Mo_7^{VI}$ in the other and (2) $Mo_4^{V}Mo_8^{VI}$ in both POMs. In the first case, both layers would be neutral whereas in the second case layer I would be anionic and layer II would be cationic. Since there are no similar 2D layers known to date, it is very difficult to determine which is the actual one. Nevertheless, ESR measurements (see below) suggest that the 3/9 + 5/7 distribution is the most realistic one.

Thus, the discrete neutral centrosymmetric units in layer I can be formulated as $[Co(phen)_2(OH)]_2[PMo_9^{VI}Mo_3^{V}O_{40}(V^{IV}O)_2]$ (Fig. 3a) whereas layer II can be formulated as $[Co(phen)_2]_2[PMo_7^{VI}Mo_5^{V}O_{40}(V^{IV}O)_2]$ (Fig. 3b).

The discrete neutral clusters forming layer I are very similar to those observed in compounds **1** and **2**: they are formed by bicapped Keggin anions $[PMo_9^{VI}Mo_3^{V}O_{40}(V^{IV}O)_2]^{2-}$ linked to two $[Co(phen)_2(OH)]^+$ cations. The bicapped Keggin POM is very similar to those found in compounds **1** and **2** (see above). The cobalt (II) ions present a distorted octahedral geometry formed by the bridging oxygen atom, O21 (Co1–O21 = 2.063(7) Å), a hydroxide anion, *cis* to the bridging O21 atom (Co1–O1W = 2.143(9) Å) and four N atoms from two phenantroline ligands (N1–N4) with very similar Co1–N bond distances (2.100(1)–2.128(9) Å) (Fig. 3a). All the *cis* angles around the cobalt (II) atom are close to 90° (78.2(4)–101.5(4)°) and the three *trans* angles are close to 180° (169.7(3)°, 172.2(4)° and 177.1(4)°). As in compounds **1** and **2**, the bridge between the POM and the Co(II) ion deviates from linearity (V1–O21–Co1 = 140.8(4)°).

Layer II is more original since it consists of an extended square lattice formed by $[Co(phen)_2]^{2+}$ cations and $[PMo_7^{VI}Mo_5^{V}O_{40}(V^{IV}O)_2]^{4-}$ anions. Each cation is linked to two POM anions and each POM anion is connected to four cations (Fig. 3b) to form an extended square lattice (Fig. 4b). The cobalt atoms (Co2) present an octahedral geometry formed by two oxygen atoms from two different POM clusters (O31 and O35) and four N atoms from two phenantroline ligands. The bridging oxygen atoms, O31 and O35, are located in *cis* (O31–Co2–O35 = 94.5(3)°) and connect the Co2 atom with a vanadium atom (V2) of one POM (Co2–O35 = 2.054(7) Å) and with a molybdenum atom (Mo7) of a different POM (Co2–O31 = 2.236(7) Å) (Table 4). Thus, each POM is linked to four cobalt ions through two V–O–Co bridges (V2–O35–Co2 = 160.7(4)°) and through two Mo–O–Co bridges (Mo7–O31–Co2 = 144.2(4)°) (Figs. 3b and 4b). The general features of the POM are very similar to those of the discrete clusters of Layer I, and those found in compounds **1** and **2** (see above). The distance between two consecutive layers of type II is about 17 Å (Fig. 5).

An interesting feature in the three compounds is that the skeletons of the Keggin POMs are fully maintained. In comparison with other bicapped Keggin POMs, this is an unusual feature. The maintenance of skeletons of Keggin POMs seemed to be simple, but it turned out to be a challenging goal under hydrothermal conditions. The successful syntheses of compounds **1**–**3** show that target synthesis of Keggin POM-based compounds can be done under hydrothermal conditions by tuning reaction conditions.

3.2. IR spectra, XPS spectra, TG analysis

The IR spectra exhibit the characteristic peaks of the α-Keggin structure at 947, 846, 792 and 898 cm^{-1} in compound **1**; 951, 869, 724 and 798 cm^{-1} in compound **2**, and 950, 842, 794 and 1055 cm^{-1} in compound **3**, attributed to $\nu(M–O_t)$, $\nu(M–O_b–M)$, $\nu(M–O_c–M)$ (M = V or Mo) and $\nu(X–O)$ (X = Si, Ge or P), respectively. The peaks at 1624,

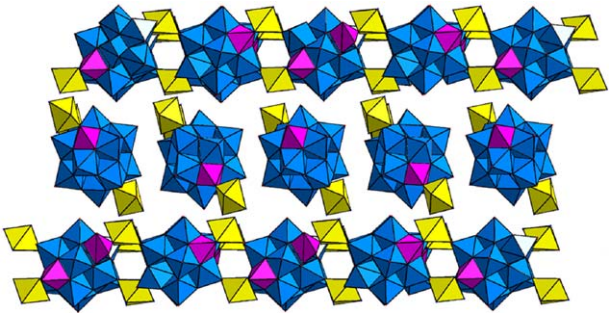

Fig. 5. Packing of the structure of **3** showing the 2D layers and the discrete POM clusters down the *b*-axis.

1518, 1494, and 1427 in compound **1**, 1627, 1519, 1455 and 1428 cm^{-1} in compound **2** and 1638, 1514, 1457 and 1429 cm^{-1} in compound **3**, are characteristic of the ligand phenantroline (Fig. S1).

The XPS spectra show a peak at 516.1 eV for **1**, 516.6 eV for **2** and 516.5 eV for **3**, that can be attributed to V(IV) [15], along with two overlapped peaks at 232.4 and 231.1 eV for **1**, 232.3 and 230.9 eV for **2**, and 232.2 and 231.2 eV for **3**, attributed to Mo(VI) and Mo(V) [16], respectively (Fig. S2). All these results further confirm the structure analysis.

The TGA show one step of weight loss for compound **1** and two steps for compounds **2** and **3** (Fig. S3). The weight loss at 260–610 °C observed in compound **1** (29.91%) is ascribed to decomposition of the phenantroline ligands (calc. 32.84%). In compound **2**, the first weight loss at 70–280 °C (1.47%) is assigned to the loss of lattice and coordinated water molecules (calc. 1.56%), and the second weight loss at 280–520 °C (25.54%) is ascribed to decomposition of the phenantroline ligands (calc. 24.90%). In compound **3**, the first weight loss at 70–260 °C (1.51%) is assigned to the loss of lattice and coordinated water molecules (calc. 1.43%), and the second weight loss at 260–570 °C (26.46%) is ascribed to the decomposition of the phenantroline ligands (calc. 25.41%).

3.3. Cyclic voltammetry

The three compounds are insoluble in water and most organic solvents, so we used them as modifiers to fabricate chemically modified CPE. CPE is a mixture of modifier, graphite powder and pasting liquid, which has been widely applied in electrochemistry because of its low cost and simplicity to prepare. In the three compounds, the Keggin skeletons are maintained (except for the addition of the two $(VO)^{2+}$ groups) and, therefore, they are expected to keep similar electrochemical properties to those of the parent Keggin POMs. For comparison purposes, we have also prepared the CPE of the insoluble salt $[(C_4H_9)_4N]_4[SiMo_{12}O_{40}]$ (**4**), containing the parent Keggin anion used in the synthesis of compound **1**. The electrochemical behavior of **1**–**4** was studied under identical conditions.

Fig. 6 shows the typical CV of **1**-CPE and **4**-CPE in a 0.2 M $Na_2SO_4+H_2SO_4$ solution (pH = 2.9) at different scan rates. Compound **1** shows three reversible redox peaks in the potential range from +600 to −500 mV with mean peak potentials $E_{1/2}=(E_{cp}+E_{ap})/2$ of +103, −48 and −224 mV (Fig. 6a). This CV is very similar to that of **4**-CPE, containing the parent POM $[(C_4H_9)_4N]_4[SiMo_{12}O_{40}]$: $E_{1/2}=+112$, −44 and −214 mV (Fig. 6b). Each reversible redox peak can be ascribed to a two-electron process of molybdenum. When the scan rate is increased, the cathodic peaks (E_{cp}) shift toward negative potentials and the corresponding anodic peaks (E_{ap}) toward positive potentials; therefore, the peak-to-peak separation between the corresponding cathodic and anodic peaks increases with the scan rate. This is a common phenomenon for CPE and may be explained as follows: the reduction of compound **1** immobilized in the CPE is accompanied by the evolution of protons from solution to maintain charge neutrality, as observed for other POMs [17]. Since the encapsulation of compound **1** in the CPE decreases the penetration rate of protons from the solution, also the electron exchange rate should be decreased, i.e., the electron exchange rate between insoluble solid **1** and the electrode is slower than that between the corresponding soluble POM and the electrode.

Fig. 6c illustrates the comparative CV of **1**-CPE and **4**-CPE in a 0.2 M $Na_2SO_4+H_2SO_4$ solution (pH = 2.9) at a scan rate of 50 mV s^{-1}. The electrochemical behaviors of **1**-CPE and **4**-CPE are very similar except for the negative shifts for the Mo(VI) reduction peak potentials in **1**-CPE compared with those of **4**-CPE. This similarity can be explained as follows: (1) In compound **1**, the skeleton of the Keggin POM is maintained, so the structural differences between **1** and **4** have very little influence on the electrochemical behavior. (2) The VO^{2+} caps have a slight effect on the electrochemical properties of compound **1**.

The cyclic voltammetric behaviors of **2**- and **3**-CPE are similar to that of **1**-CPE: they also show three pairs of reversible redox peaks that present the same kind of shift in the cathodic and anodic potentials with increasing scan rates (Fig. S4). As expected, none of the three compounds shows reduction of the "grafting" metallic cations (Cu, Zn, Co and V) in the potential range studied.

Clinton et al. have systematically studied the electrochemical behavior of V^{n+} in $[PV^{n+}W_{11}O_{40}]^{(n-9)-}$ ($n=3$, 4, and 5), showing reversible interconversion between V^{3+}, V^{4+} and V^{5+}, in the 200–850 mV range [18]. However, in compounds **1**–**3**, no redox waves of V^{n+} can be observed. Two reasons may explain this different electrochemical behavior: (1) the electrochemical behavior occurs in different phases (in solution for $[PV^{n+}W_{11}O_{40}]^{(n-9)-}$ and in solid state for compounds **1**–**3**) and (2) the geometric environments of the V centers are different. Thus, all the V atoms in $[PV^{n+}W_{11}O_{40}]^{(n-9)-}$ are in octahedral geometry and reversible interconversions between V^{3+}, V^{4+} and V^{5+} are accompanied by slight geometric changes of the VO_6 octahedra. In compounds **1**–**3**, the V atoms are in a

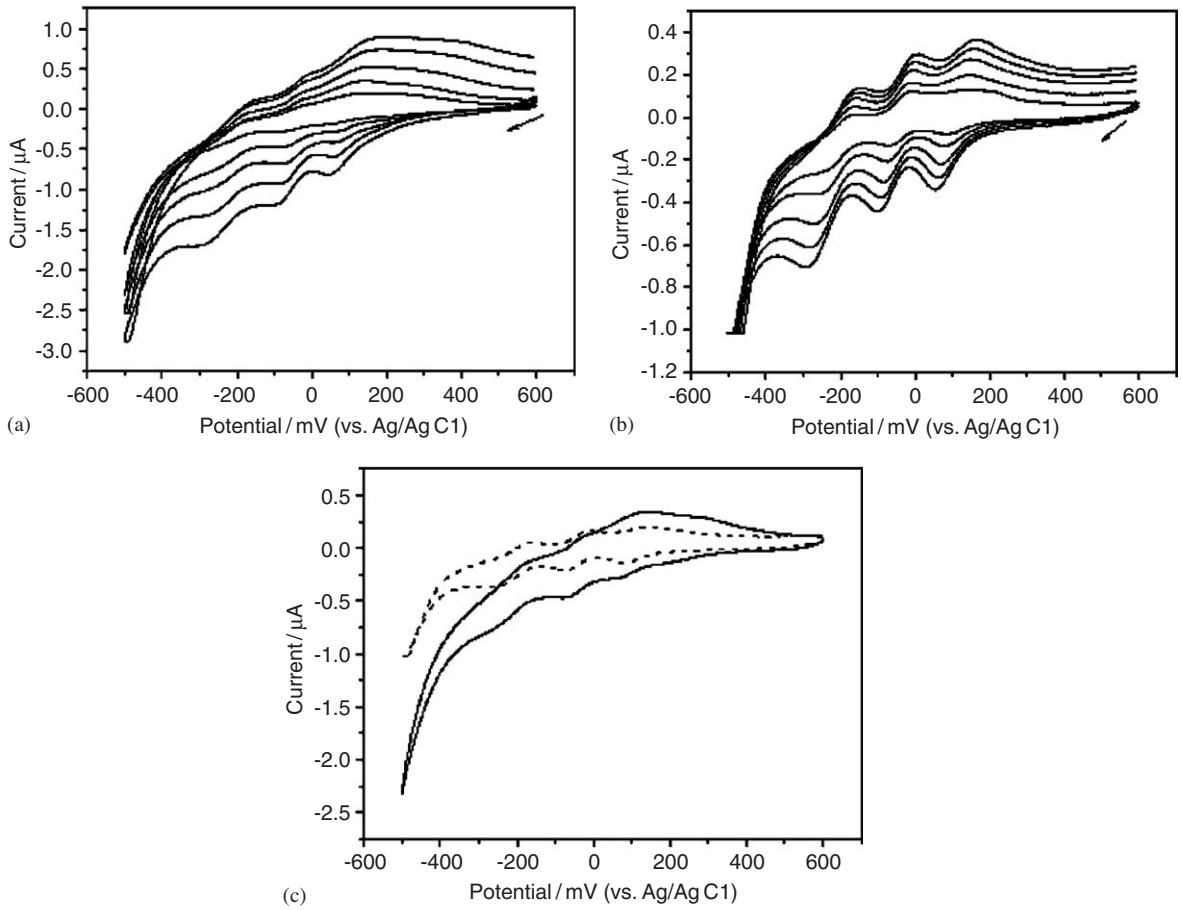

Fig. 6. Cyclic voltammograms in a 0.2 M $Na_2SO_4 + H_2SO_4$ solution (pH = 2.9) at different scan rates (from inner to outer: 20, 50, 100, 150 and 200 mV s^{-1}) of: (a) **1**-CPE and (b) **4**-CPE (c) Comparative cyclic voltammograms of **1**-CPE (solid line) and **4**-CPE (dotted line) in a 0.2 M $Na_2SO_4 + H_2SO_4$ solution (pH = 2.9) at a scan rate of 50 mV s^{-1}. Potentials measured vs. Ag/AgCl.

$\{VO_5\}$ square pyramidal environment with one short V–O_t bond and four longer V–O_b bonds. Furthermore, the O_t atoms are covalently bound to the phenantroline metallic complexes. The reduction or oxidation of the V^{4+} centers should imply geometric changes of the $\{VO_5\}$ group from square pyramidal into octahedral, probably resulting in the collapse of the whole POM structure.

In addition, POMs are very sensitive to pH and therefore changes in the pH are expected to affect the electrochemical properties of POMs. Fig. 7 shows the electrochemical behavior of **2**-CPE in a 0.2 M $Na_2SO_4 + H_2SO_4$ aqueous solution with different pH's at a scan rate of 50 mV s^{-1}. We can see that all the peaks gradually shift towards more positive potentials, the peak currents increase when decreasing the pH and a new pair of waves appears at pH = 2.6, probably due to acid-catalized decomposition [19].

3.4. Magnetic properties

The thermal variation of the product of the molar magnetic susceptibility times the temperature, $\chi_m T$, for the three compounds shows room temperature values of 1.6, 2.0 and 14.4 emu K mol^{-1} for **1**, **2** and **3**, respectively (Fig. 8). On lowering the temperature, compounds **1** and **2** show similar behaviors: the $\chi_m T$ product smoothly decreases, reaching a plateau between ca. 5 and 30 K with $\chi_m T$ values of ca. 0.8 and 1.5 emu K mol^{-1}, respectively. Below ca. 5 K both compounds show a more abrupt decrease, reaching, at 2 K, $\chi_m T$ values of ca. 0.75 and 1.35 emu K mol^{-1}, respectively. The magnetic behavior of compound **3** is also similar: the $\chi_m T$ product shows a smooth decrease on lowering the temperature, although there is no plateau at low temperatures. Below ca. 40 K the $\chi_m T$ product shows a more abrupt decrease, reaching, at 2 K, a $\chi_m T$ value of ca. 8.0 emu K mol^{-1} (Fig. 8).

The room temperature values for the three compounds (1.6, 2.0 and 14.4 emu K mol^{-1} for **1**, **2** and **3**, respectively) are clearly below the expected values of 2.25, 4.50 and ca. 16–19 emu K mol^{-1}, calculated for the spin-only values of the uncoupled $S = 1/2$ Mo(V) (four, eight and ten in **1**, **2** and **3**, respectively) plus the uncoupled $S = 1/2$ V(IV) (two in **1** and four in **2** and **3**) plus the four $S = 3/2$ Co(II) ions (in **3**). Note that the magnetic contribution of each Co(II) ions is expected to be between 2.7 and 3.4 emu K mol^{-1}, the usual range given for high-spin octahedral monomeric

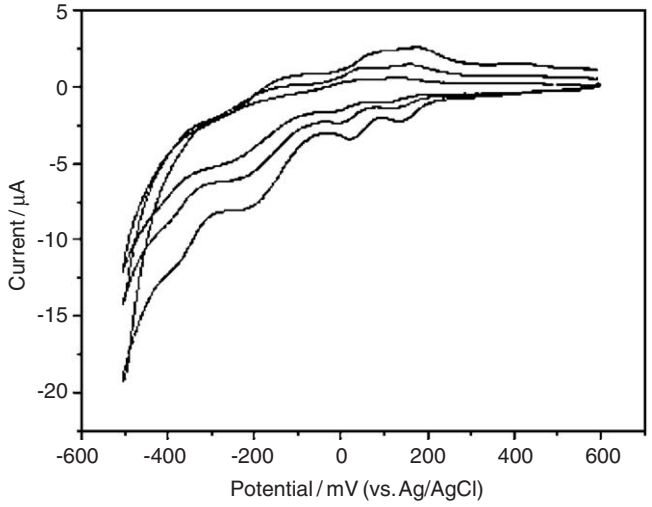

Fig. 7. Cyclic voltammograms of **2**-CPE in a 0.2 M $Na_2SO_4+H_2SO_4$ aqueous solution at different pH values (from inner to outer: pH = 3.1, 2.9 and 2.6) at a scan rate of 50 mV s^{-1}.

complexes [20]. The differences observed between the experimental and the calculated room temperature $\chi_m T$ values and the continuous decrease shown by the $\chi_m T$ product from room temperature indicate that there exists a strong antiferromagnetic coupling between the Mo(V) in the three structures and that at low temperatures these delocalized electrons are completely paired. In fact, at low temperatures the $\chi_m T$ product of compounds **1** and **2** reaches a plateau of ca. 0.8 and 1.5 emu K mol^{-1}, respectively, in agreement with the expected values for the contributions of the two and four $S = 1/2$ V(IV) ions present in **1** and **2**, respectively. This spin pairing of the delocalized electrons has already been observed in many other reduced POMs with several Mo(V) and/or V(IV) ions in their structures [4]. In compounds **1** and **2** the weak, although more abrupt, decrease of the $\chi_m T$ product below ca. 5 K may indicate the presence of very weak antiferromagnetic interactions between the V(IV) atoms in the POMs, taking place, probably, via the delocalized electrons of the POM skeleton. Note that in compound **3** the decrease of the $\chi_m T$ product from room temperature is also due to the spin–orbit coupling present in octahedral Co(II) complexes [20,21]. In this compound **3**, the more abrupt decrease observed below ca. 40 K may be attributed to a zero field splitting present in the Co(II) ions and/or to the presence of weak antiferromagnetic exchange interactions between the Co(II) and the V(IV) ions via the bridging oxygen atom connecting these two ions, as can be anticipated from the almost linear V–O–Co bridges. Unfortunately, due to the many possible magnetic exchange schemes and their complexity, it is not possible to fit the magnetic data with any available model.

The spin pairing and the weak magnetic contributions of the delocalized electrons in the POM skeletons preclude the determination of the number of reduced Mo(V) ions in

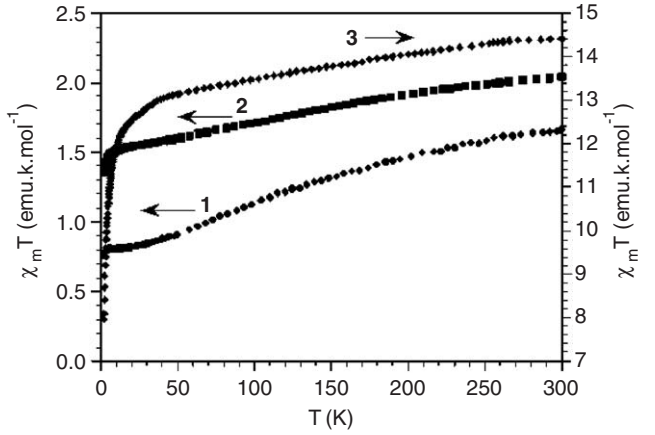

Fig. 8. Thermal variation of the product of the magnetic susceptibility times the temperature, $\chi_m T$, for the three compounds.

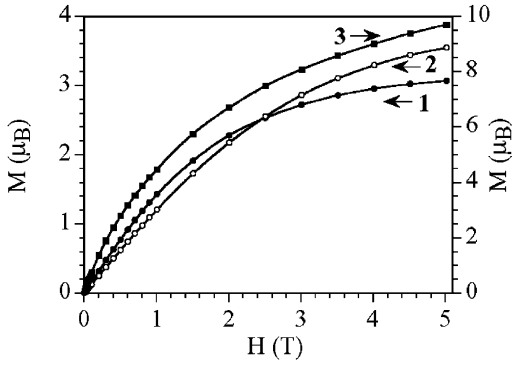

Fig. 9. Isothermal magnetization at 2 K of the three compounds.

each POM cluster and, therefore, the only proofs of the proposed formulas are the charge balance and the BVS calculations (see above).

Finally, isothermal magnetization measurements at 2 K show saturation values of ca. 3.0, 3.5 and 10.0 μ_B for compounds **1**–**3**, respectively (Fig. 9). These values are below those expected for the corresponding spin-only systems (see above) and confirm the presence of strong antiferromagnetic interactions within the Mo(V) atoms in the POMs.

The ESR spectrum of compound **3** at room temperature shows two groups of eight signals centered at $g \approx 2$, typical of the ($V^{IV}O$) group (Fig. 10) [22]. These two groups correspond to the parallel ($g_{||}$) and perpendicular ($g_{\perp}$) components of the resonance of the unpaired electron located on the V(IV) atom. The splitting of these two components into eight lines arises from the hyperfine coupling of the unpaired electron with the ^{51}V(IV) nucleus ($I = 7/2$, natural abundance = 99.75%). The analysis of the two groups of eight lines gives the following parameters: $g_{||} = 1.9393$, $A_{||} = 174$ G $= 1.58 \times 10^{-2}$ cm^{-1}, $g_{\perp} = 1.9700$ and $A_{\perp} = 60$ G $= 5.52 \times 10^{-3}$ cm^{-1} (Fig. 10). These values are very similar to those found in other VO^{2+} complexes with similar environments [22]. From the weak intensity of the two eight-lines groups (in fact, at low

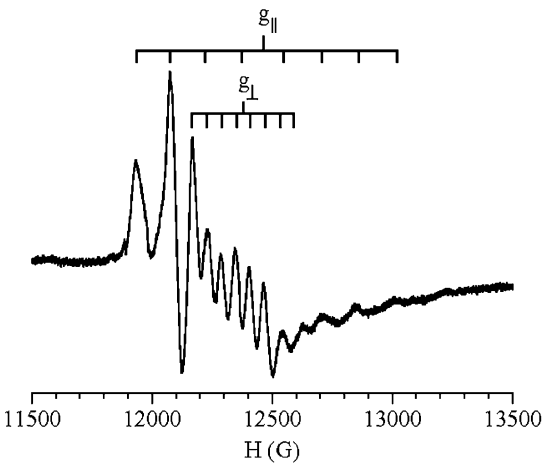

Fig. 10. Q-band ESR spectrum at room temperature of compound **3**.

temperatures they become negligible compared with those of the Mo(V) centers, see below), we can deduce that they might be originated by a small amount of POM clusters containing $(VO)^{2+}$ groups not linked to the cobalt complexes. This observation supports the presence of antiferromagnetic exchange interactions between the V(IV) and the Co(II) centers observed in the magnetic measurements. Furthermore, no signal from the Mo(V) ions could be observed at high temperatures, indicating that the electrons are delocalized over all the Mo atoms of the POM skeleton. This situation is very common in reduced POMs, which are ESR silent at high temperatures [23]. Note that there are five delocalized electrons in the POM skeleton of compound **3** and, therefore, even in the case of a complete spin pairing of the delocalized electrons, there should be at least one unpaired electron in the POM skeleton.

When lowering the temperature, the ESR spectra of compound **3** become more complicated since new features appear at $g \approx 2$ below ca. 120 K, overlapping with those of the $(VO)^{2+}$ group (Fig. 11). Fortunately, at very low temperatures the signals from the $(VO)^{2+}$ group became almost negligible and, thus, a close look at the features appearing at low temperature shows the presence of a main signal, centered at $g = 1.946$, which appears split into 6 lines with a separation of ca. 130 G. This splitting is due to the hyperfine coupling of the unpaired electron with the ^{95}Mo and ^{97}Mo nuclei ($I = 5/2$, natural abundances of 15.9% and 9.6%, respectively) and indicates that this signal arises due to the progressive localization of the unpaired electron in the Mo atoms of the POM skeleton. [23]. Furthermore, the intensity of the Mo(V) signal increases when lowering the temperature following a Curie law, as expected for a signal coming from a localized unpaired electron. This behavior indicates that there is an odd number of delocalized electrons in at least one of the two POMs and, therefore, that the Mo(V)/Mo(VI) ratios in the two POMs must be 3/9 and 5/7 rather than 4/8 for both (see above).

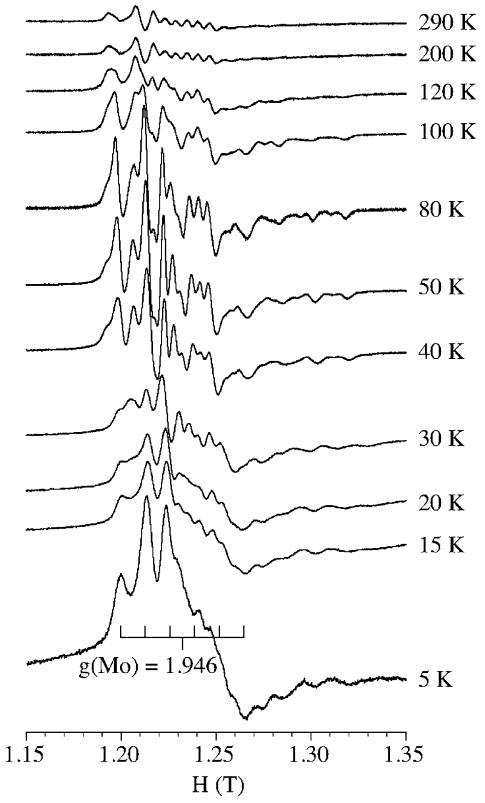

Fig. 11. Thermal variation of the Q-band ESR spectrum of compound **3**.

4. Conclusion

Three new Keggin POM-based compounds have been hydrothermally synthesized by directly using classical Keggin polyoxoanions as building blocks. Compound **1** consists of one crystallographically unique bicapped Keggin cluster connected to two (phen)copper(I) complexes, with two bis(phen)copper(I) complexes as counterions. Compound **2** contains two kinds of bicapped Keggin clusters linked to two very similar bis(phen)zinc(II) complexes, whereas compound **3** is a two-dimensional POM-based network formed by bicapped Keggin anions connected through bis(phen)cobalt(II) complexes. This work evidences that the coordination preference of the metal ions plays a key role in the dimensionality of the final crystal structure of the Keggin POM-based solids and that it is possible to synthesize, under hydrothermal conditions, new Keggin POM-based compounds by using preformed Keggin POMs. Further research is underway to provide more examples and information about the influence of other different metal ion complexes on the structures of POM-based compounds and to explore their physical properties.

Acknowledgments

This research was financially supported by the National Science Foundation of China (20271011) and by the Spanish Generalitat Valencia (projects GV04B-078 and

IIARC0/2004/159). The authors also thank the reviewers for their excellent comments for improving the manuscript.

References

[1] (a) V. Soghomonian, Q. Chen, R.C. Haushalter, J. Zubieta, Science 259 (1993) 1596;
(b) Z. Shi, S.H. Feng, S. Gao, L.R. Zhang, G.Y. Yang, J. Hua, Angew. Chem. Int. Ed. 39 (2000) 2325;
(c) O.M. Yaghi, M. O'Keeffe, N.W. Ockwig, H.K. Chae, M. Eddaoudi, J. Kim, Nature 423 (2003) 705;
(d) P.S. Halasyamani, M.J. Drewitt, D. O'Hare, Chem. Commun. (1997) 867;
(e) Y. Wang, J.H. Yu, Y. Du, Z. Shi, Y.C. Zou, R.R. Xu, J. Chem. Soc., Dalton Trans. (2002) 4060;
(f) A. Müller, F. Peters, M.T. Pope, D. Gatteschi, Chem. Rev. 98 (1998) 239.

[2] (a) E. Coronado, C.J. Gómez-García, Chem. Rev. 98 (1998) 273;
(b) P. Gouzerh, A. Proust, Chem. Rev. 98 (1998) 77;
(c) E. Coronado, J.R. Galan-Mascaros, C. Giménez-Saiz, C.J. Gómez-García, E. Martinez-Ferrero, M. Almeida, E.B. Lopes, S.C. Capelli, R.M. Llusar, J. Mater. Chem. 14 (2004) 1867;
(d) E. Coronado, C. Giménez-Saiz, C.J. Gómez-García, S.C. Capelli, Angew. Chem. Int. Ed. 43 (2004) 3022.

[3] (a) A. Müller, P. Kögerler, Coord. Chem. Rev. (2000) 335;
(b) P.J. Hagrman, D. Hagrman, J. Zubieta, Angew. Chem. Int. Ed. 38 (1999) 2638;
(c) X.Y. Wei, M.H. Dickman, M.T. Pope, J. Am. Chem. Soc. 120 (1998) 10254;
(d) Y.G. Wei, B.B. Xu, C.L. Barnes, Z.H. Peng, J. Am. Chem. Soc. 123 (2001) 4083.

[4] (a) E. Burkholder, V. Golub, C.J. O'Connor, J. Zubieta, Inorg. Chem. 42 (2003) 6729;
(b) L.M. Duan, C.L. Pan, J.Q. Xu, X.B. Cui, F.T. Xie, T.G. Wang, Eur. J. Inorg. Chem. (2003) 2578;
(c) M. Yuan, Y.G. Li, E.B. Wang, C.G. Tian, L. Wang, C.W. Hu, N.H. Hu, H.Q. Jia, Inorg. Chem. 42 (2003) 3670;
(d) S.T. Zheng, J. Zhang, G.Y. Yang, Eur. J. Inorg. Chem. (2004) 2004;
(e) J.Y. Niu, D.J. Guo, J.P. Wang, J.W. Zhao, Cryst. Growth Des. (2004) 241;
(f) W.B. Yang, C.Z. Lu, Inorg. Chem. 41 (2002) 5638;
(g) D. Drewes, E.M. Limanski, B. Krebs, Eur. J. Inorg. Chem. (2004) 4849;
(h) C.M. Liu, D.Q. Zhang, M. Xiong, D.B. Zhu, Chem. Commun. (2002) 1416;
(i) C.M. Liu, J.L. Luo, D.Q. Zhang, N.L. Wang, Z.J. Chen, D.B. Zhu, Eur. J. Inorg. Chem. (2004) 4774;
(j) F.Y. Li, L. Xu, Y.G. Wei, E.B. Wang, Inorg. Chem. Commun. 8 (2005) 263;
(k) C.M. Liu, D.Q. Zhang, C.Y. Xu, D.B. Zhu, Solid State Sci. 6 (2004) 689.

[5] (a) J.R. Galán-Mascarós, C. Gimenez-Saiz, S. Triki, C.J. Gómez-García, E. Coronado, L. Ouahab, Angew. Chem. Int. Ed. 34 (1995) 1460;
(b) E. Coronado, J.R. Galán-Mascarós, C. Giménez-Saiz, C.J. Gómez-García, S. Triki, J. Am. Chem. Soc. 120 (1998) 4671.

[6] R.L. LaDuc Jr., R.S. Rarig Jr., P.J. Zapf, J. Zubieta, Inorg. Chim. Acta 292 (1999) 131.

[7] P.J. Hagrman, R.L. Laduca, H.J. Koo, R. Rarig, J.R.C. Haushalter, M.H. Whangbo, J. Zubieta, Inorg. Chem. 39 (2000) 4311.

[8] L. Pan, T. Frydel, M.B. Sander, X.Y. Huang, J. Li, Inorg. Chem. 40 (2001) 1271.

[9] Z.Y. Shi, X.J. Gu, J. Peng, E.B. Wang, J. Mol. Struct. (2005) 147.

[10] X.J. Gu, J. Peng, Z.Y. Shi, Y.H. Chen, Z.G. Han, E.B. Wang, J.F. Ma, Inorg. Chim. Acta 358 (2005) 3701.

[11] C.R. Deltcheff, M. Fournier, R. Franck, R. Thouvenot, Inorg. Chem. 22 (1983) 207.

[12] G.Y. Luan, Y.G. Li, E.B. Wang, Z.B. Han, C.W. Hu, N.H. Hu, H.Q. Jia, Inorg. Chem. Commun. 5 (2002) 509.

[13] Q. Chen, C.L. Hill, Inorg. Chem. 35 (1996) 2403.

[14] I.D. Brown, D. Altermatt, Acta Crystallogr. B 41 (1985) 244.

[15] A.I. Minyaev, I.A. Denisov, V.E. Soroko, V.A. Konovalov, Z. Prikl Khim 59 (1986) 339.

[16] T.A. Patterson, J.C. Carver, D.E. Leyden, D.M. Hercules, J. Phys. Chem. 80 (1976) 1702.

[17] M.T. Pope, E. Papaconstantinou, Inorg. Chem. 6 (1967) 1147.

[18] D.E. Clinton, D.A. Tryk, I.T. Bae, F.L. Urbach, M.R. Antonio, D.A. Scherson, J. Phys. Chem. 100 (1996) 18511.

[19] B. Keita, L. Nadjo, J. Electroanal. Chem. 227 (1987) 77.

[20] R. March, W. Clegg, R.A. Coxall, L. Cucurull-Sánchez, L. Lezama, T. Rojo, P. González-Duarte, Inorg. Chim. Acta 353 (2003) 129.

[21] O. Kahn, Molecular Magnetism, Wiley-VCH, New York, 1993.

[22] B.A. Goodman, J.B. Raynor, Adv. Inorg. Chem. Radiochem. (1970) 135.

[23] E. Coronado, J.R. Galán-Mascarós, C. Giménez-Saiz, C.J. Gómez-García, L.R. Falvello, P. Delhaes, Inorg. Chem. 37 (1998) 2183 (and references therein).